ASN NEURO RESEARCH ARTICLE

ASN NEURO 4(6):art:e00101.doi:10.1042/AN20120045

The palmitoylation state of PMP22 modulates epithelial cell morphology and migration

Susie J. Zoltewicz*, Sooyeon Lee*, Vinita G. Chittoor*, Steven M. Freeland*, Sunitha Rangaraju*, David A. Zacharias*,† and Lucia Notterpek*[1]

*Department of Neuroscience, College of Medicine, McKnight Brain Institute, University of Florida, Gainesville, FL 32610, U.S.A.
†The Marine Whitney Laboratories, University of Florida, St. Augustine, FL 32080, U.S.A.

Cite this article as: Zoltewicz SJ, Lee S, Chittoor VG, Freeland SM, Rangaraju S, Zacharias DA and Notterpek L (2012) The palmitoylation state of PMP22 modulates epithelial cell morphology and migration. ASN NEURO 4(6):art:e00101.doi:10.1042/AN20120045

ABSTRACT

PMP22 (peripheral myelin protein 22), also known as GAS 3 (growth-arrest-specific protein 3), is a disease-linked tetraspan glycoprotein of peripheral nerve myelin and constituent of intercellular junctions in epithelia. To date, our knowledge of the post-translational modification of PMP22 is limited. Using the CSS-Palm 2.0 software we predicted that C85 (cysteine 85), a highly conserved amino acid located between the second and third transmembrane domains, is a potential site for palmitoylation. To test this, we mutated C85S (C85 to serine) and established stable cells lines expressing the WT (wild-type) or the C85S-PMP22. In Schwann and MDCK (Madin–Darby canine kidney) cells mutating C85 blocked the palmitoylation of PMP22, which we monitored using 17-ODYA (17-octadecynoic acid). While palmitoylation was not necessary for processing the newly synthesized PMP22 through the secretory pathway, overexpression of C85S-PMP22 led to pronounced cell spreading and uneven monolayer thinning. To further investigate the functional significance of palmitoylated PMP22, we evaluated MDCK cell migration in a wound-healing assay. While WT-PMP22 expressing cells were resistant to migration, C85S cells displayed lamellipodial protrusions and migrated at a similar rate to vector control. These findings indicate that palmitoylation of PMP22 at C85 is critical for the role of the protein in modulating epithelial cell shape and motility.

Key words: lipid modification, myelin, protein trafficking, Schwann cell, tetraspan.

INTRODUCTION

PMP22 (peripheral myelin protein 22), also known as GAS 3 (growth-arrest-specific protein 3), is a tetraspan glycoprotein most studied for its linkage to hereditary demyelinating peripheral neuropathies (Pareek et al., 1997; Houlden and Reilly, 2006). PMP22/GAS 3 has also been implicated in cancers of various tissue origin (Huhne et al., 1999; van Dartel et al., 2002; Li et al., 2005; Mimori et al., 2005), in schizophrenia (Dracheva et al., 2006), in major depression (Aston et al., 2004), and was identified as a promising biomarker for mood disorders (Le-Niculescu et al., 2008). Despite these associations with disease states and the increasing relevance of PMP22 to human health, the function of the protein remains incompletely understood. In a variety of cell types, overexpression of PMP22 has been shown to affect cellular morphology and lead to membrane protrusions by unknown mechanisms (Brancolini et al., 1999). In endothelia and epithelia, PMP22 is a constituent of intercellular junctions and its expression level affects the barrier property of the monolayer (Notterpek, 2001; Roux et al., 2004, 2005). In Schwann cells, PMP22 is involved in the extensive morphological and organisational changes of the plasma membrane that occur during myelination, as in the absence of PMP22 the cells do not form normal myelin (Adlkofer et al., 1995; Amici et al., 2007). How PMP22 might impact these diverse cellular functions is not known but likely involves post-translational modifications of the protein.

S-palmitoylation is a reversible, post-translational modification in which the 16-carbon saturated lipid palmitate is covalently added to cysteine residues via a thiolester linkage (Linder and Deschenes, 2007). Palmitoylation is known to affect protein trafficking and sorting, protein stability,

[1] To whom correspondence should be addressed (email notterpek@ufl.edu)

Abbreviations: Con A, concavalin A; C85, cysteine 85; C85S, C85 to serine; Endo H, endoglycosidase H; ER, endoplasmic reticulum; GAPDH, glyceraldehyde-3-phosphate dehydrogenase; GAS3, growth-arrest-specific protein 3; GFP, green fluorescent protein; HA, haemagglutinin; HN, hydroxylamine; HRP, horseradish peroxidase; MDCK, Madin–Darby canine kidney; ODYA, octadecynoic acid; PLP, proteolipid protein; Palm-YFP, palmitoylatable yellow fluorescent protein; PMP22, peripheral myelin protein 22; PNGaseF, peptide *N*-glycosidase F; RIPA, radioimmunoprecipitation assay; TX-100, Triton X-100; VVL, *Vicia villosa* lectin; WT, wild-type.

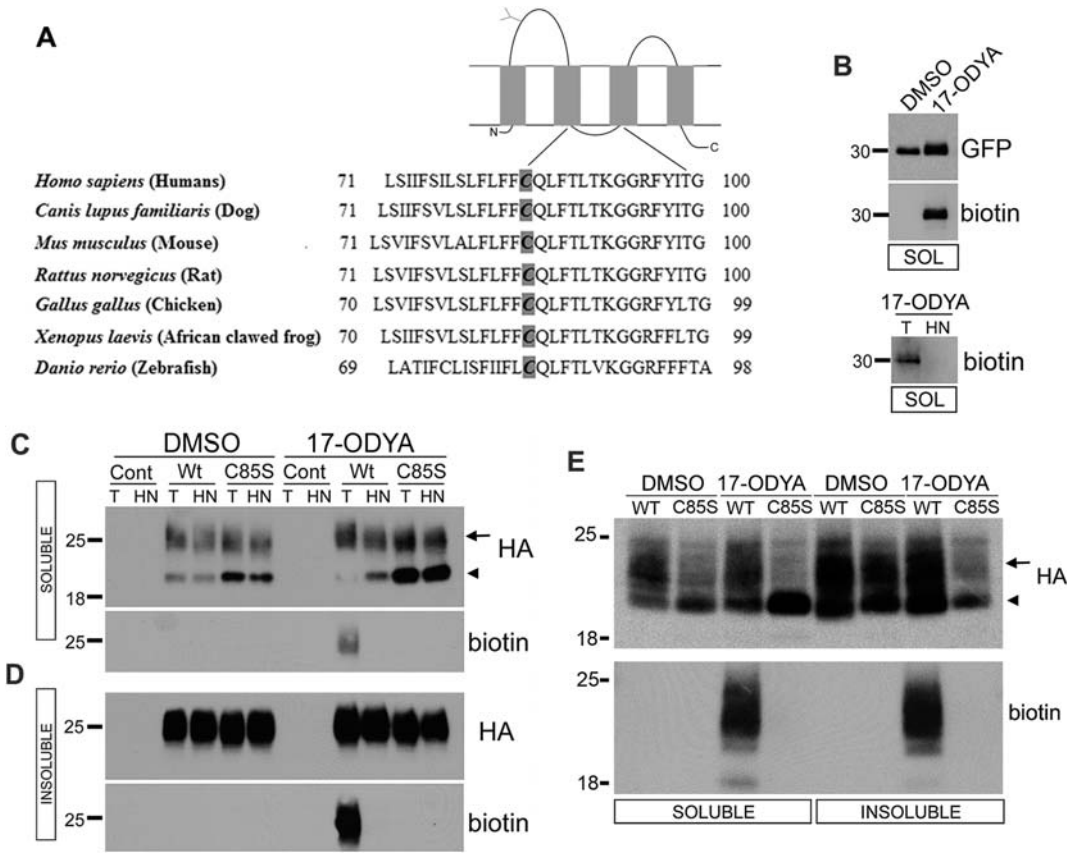

Figure 1 **PMP22 is palmitoylated at C85**

Diagrammatic representation of PMP22 (top) with the conserved region surrounding C85 across species (**A**). Palm-YFP (**B**), parental control (Cont), or WT and C85S-PMP22 expressing MDCK (**B–D**) or Schwann (**E**) cells were metabolically labelled with the palmitate analogue 17-ODYA or DMSO vehicle (**B–E**). YFP (**B**) or PMP22 (**C–E**) were immunoprecipitated from RIPA buffer-soluble (**B, C, E**) and -insoluble (**D, E**) extracts. Immunoprecipitates were reacted with biotin azide, and equal portions were treated with either Tris (T) or HN and processed for blotting. The same blot was probed sequentially for 17-ODYA (biotin) and then for Palm-YFP (GFP) or PMP22 (HA). Palmitoylation of WT-PMP22 is detected as a broadband of biotinylated proteins near 25 kDa (arrows), which is removed by HN, but not by Tris (T) treatment. Arrowheads in the MDCK and Schwann cell samples mark the migration position of the immature, Endo H-sensitive PMP22. Palmitoylation is absent in C85S-PMP22 expressing cultures. Molecular mass, in kDa.

protein–protein and protein–lipid interactions, and functions such as cell spreading, signalling and migration (Hemler, 2003; Yang, 2004; Zhou et al., 2004; Schneider, 2005; Greaves and Chamberlain, 2007; Linder and Deschenes, 2007). Tetraspan membrane proteins like the claudins, to which PMP22 has significant amino acid similarity, can be palmitoylated at membrane-proximal cysteine residues (Van Itallie, 2005). PMP22 contains one juxtamembrane cysteine at residue 85, which is located in the cytoplasmic region between the second and third transmembrane domains. Based on BLAST searches, this cysteine residue is conserved in PMP22 orthologues among vertebrates, including humans, mammals, chicken (*Gallus gallus*), frogs (*Xenopus laevis* and *tropicalis*) and zebrafish (*Danio rerio*) (Figure 1A), underscoring its likely importance.

To examine the potential palmitoylation of PMP22, we chose MDCK (Madin–Darby canine kidney) epithelia and primary rat Schwann cells, both of which are amenable to PMP22 overexpression and protein trafficking studies (Roux et al., 2005). Here, we show that while palmitoylation of PMP22 at C85 (cysteine 85) is not necessary for the maturation of the newly synthesized protein, this lipid modification has a dramatic influence on how PMP22 affects epithelial cell morphology and migration.

MATERIALS AND METHODS

Cell culture, cloning and establishment of stable cell lines

To make non-palmitoylated PMP22, a cDNA encoding the WT (wild-type) mouse protein with a human influenza HA (haemagglutinin) epitope tag sequence in the second extracellular loop in the pCMX vector was used as a template (Tobler et al.,

1999). The amino acid substitution of C85 (TGC) was changed to serine (AGC) [C85S (C85 to serine)-PMP22] using the PCR-based Quikchange kit (Stratagene). Clones were fully sequenced for verification. cDNA encoding WT or C85S-PMP22 was then subcloned into the pEFIRES-P vector (Hobbs et al., 1998). To create stable lines, MDCK type II cells were transfected on six-well plates at approximately 50% confluence using 8 μl of Lipofectamine™ 2000 (Invitrogen) and 3 μg of DNA (WT or C85S in pEFIRES-P or empty pEFIRES-P vector) in a final volume of 2 ml of medium per well. After 28 h, puromycin was added at 4 μg/ml to kill non-transfected cells. The next day, puromycin was decreased to 2 μg/ml and maintained at this level for eight additional days. Resulting colonies were pooled, expanded and either maintained for experimental analyses or frozen in aliquots. Puromycin was added to the media at 2 μg/ml for 24–48 h immediately preceding each experiment. Primary rat Schwann cells were cultured as described (Johnson et al., 2005), and transfected on 10 cm plates using 21 μl of Lipofectamine™ 2000 and 8 μg DNA. Cells were grown in DMEM (Dulbecco's modified Eagle medium) with 10% FCS (fetal calf serum) at 37°C in 5% CO_2. Confluent cultures were split on to tissue culture dishes at 1:5 and maintained using established procedures (Johnson et al., 2005).

Antibodies and fluorescent organelle markers

Antibodies used included anti-GP135 (Roux et al., 2005), anti-HA 3F10 (Roche), anti-α-tubulin (Sigma), anti-ZO1 (Invitrogen), anti-GAPDH (glyceraldehyde-3-phosphate dehydrogenase; EnCor Biotechnology Inc.), anti-GFP (green fluorescent protein; Abcam), anti-ezrin (Cell Signaling), anti-caveolin 1 (BD Biosciences) and anti-actin (Sigma). Fluorescein (FITC)-conjugated organelle markers Con A (concavalin A-FITC) and VVL (*Vicia villosa* lectin-FITC) were purchased from Vector Laboratories, and Alexa Fluor®-594-conjugated phalloidin, Lysotracker Red DND-99 and Hoechst were obtained from Invitrogen.

Labelling of palmitate via click chemistry

MDCK or rat Schwann cells transiently expressing Palm-YFP (palmitoylatable yellow fluorescent protein) (Zacharias et al., 2002), or stably expressing WT or C85S-PMP22 or no DNA (control) were labelled with 50 μM 17-ODYA (17-octadecynoic acid; Cayman Chemical. Co.) or DMSO vehicle (Sigma) overnight at 37°C. To facilitate dissolution of 17-ODYA in the medium, 37.5 μl 20 mM 17-ODYA stock in DMSO (or DMSO only) was premixed with 75 μl 10% fatty acid free BSA (Sigma–Aldrich), added to 15 ml medium, vortexed, and then 3 ml added per plate. After labelling, cells were lysed in RIPA (radioimmunoprecipitation assay) buffer, separated into detergent-soluble and -insoluble extracts, and processed for IP (immunoprecipitations) as described (Zoltewicz et al., 2009), with the following modifications. To create insoluble extracts, RIPA-insoluble pelleted material was first solubilized in 100 μl 50 mM Hepes, pH 7.0, 150 mM NaCl, 1% SDS and 10% DMSO, then diluted with 0.9 ml of SDS-free RIPA, spun for 10 min, and supernatants were transferred to clean tubes. Total protein in lysates was measured using the BCA (bicinchoninic acid) kit (Pierce). YFP or PMP22 was immunoprecipitated from the cell extracts with anti-GFP and protein G agarose (Roche) or high affinity anti-HA matrix (Roche) overnight at 4°C. After five washes, bound proteins were eluted with 25 μl of 50 mM Hepes, pH 7, 150 mM NaCl and 2% SDS. Eluates (24 μl) were transferred to fresh tubes and the following reagents added individually to perform the Cu-catalysed click reaction (Charron et al., 2009): 0.25 μl 10 mM biotin azide (Invitrogen), 0.5 μl 50 mM TCEP [Tris-(2-carboxyethyl)phosphine] hydrochloride (Thermo Fisher Scientific), 0.25 μl 10 mM TBTA {Tris[(1-benzyl-1*H*-1,2,3-triazol-4-yl)methyl]amine; Sigma} and 0.5 μl 50 mM $CuSO_4$ (Sigma). Reaction mixtures were incubated for 1 h with intermittent mixing, and then 0.5 μl of 0.5 M EDTA added to terminate the reactions. Then, 7.5 μl of each reacted eluate was mixed with an equal volume of 2 M Tris, pH 7.5 (control) or 2 M HN (hydroxylamine), pH 7.5, and incubated at 37°C for 3 h. Samples were reduced with 5 mM DTT (dithiothreitol) at 80°C for 5 min, and resolved on gels and blotted.

Immunoblotting

Cell lysates (20–25 μg per lane) were resolved using 4–12% or 12% gels in Mops buffer and NuPAGE reagents (Invitrogen), and blotted as described (Zoltewicz et al., 2009). Blots were probed sequentially for YFP with anti-GFP or for PMP22 with anti-HA and then for biotin with streptavidin-HRP (horseradish peroxidase) (Thermo Scientific). Films were digitally imaged and analysed as described (Rangaraju et al., 2010). For deglycosylation reactions, 15 μg of total cell lysates were digested with Endo H (endoglycosidase H) or PNGase F (peptide *N*-glycosidase F) (New England Biolabs) and subsequently processed for immunoblotting (Pareek et al., 1997).

Pulse-chase labelling experiments

Pulse-chase analyses were performed as described (Pareek et al., 1997; Ryan et al., 2000). Briefly, confluent cells on 6-well plates were labelled with 125 μCi/well ^{35}S-methionine and cysteine containing media for 30 min, and then chased with unlabelled media for the indicated times. RIPA buffer-soluble extracts were made from cells harvested at each time point. Protein was measured and concentrations normalized to 1 mg/ml. Then 500 μg of each sample was incubated with HA beads overnight at 4°C with mixing, then beads were washed five times with RIPA buffer. Immunoprecipitate yields were divided in half and either treated with Endo H or G5 reaction buffer (0.5% SDS, 1% 2-mercaptoethanol and 0.05 M sodium citrate, pH 5.5) alone, resolved on gels, incubated with Amplify (GE Healthcare), dried and exposed to film. Densitometric analyses of the autoradiographs were performed using NIH Image software.

Immunofluorescence microscopy and morphological measurements

Cells were seeded on to glass coverslips at a density of 3×10^5 cells per cm^2 and processed as described (Ryan et al., 2000), except the blocking buffer was PBS with 10% goat serum and cells were permeabilized for 10 min with 0.1% TX-100 (Triton X-100) in PBS at 20°C. For labelling non-permeabilized cells, the TX-100 step was omitted. For samples double-stained with mouse and rat primary antibodies, the labelling was done sequentially, and secondary antibodies specifically adsorbed against the opposite species were used to prevent cross-reactivity (goat anti-mouse min × rat DyLight 488, goat anti-rat min × mouse DyLight 594; Jackson ImmunoResearch Labs Inc.). Acidic compartments in live cells on coverslips were identified by incubation with 1 μl/ml Lysotracker Red DND-99 (Invitrogen) for 45 min at 37°C, fixed, and processed for visualization. Samples were imaged using a Spot camera mounted on a Nikon E800 microscope, or with a Hamamatsu CCD camera and an Olympus IX81-DSU spinning disk confocal microscope. Images were processed with Spot or Slidebook software followed by Adobe Photoshop and Illustrator CS.

Fully-confluent and uniform monolayers of MDCK cells on coverslips were immunostained for ZO1 as above, and four separate images were captured from similar locations on each coverslip. Images were opened using ImageJ software and the polygon tool was used to trace the ZO1 boundaries of a group of approximately 100 cells, and the software calculated the area within the outline. The number of nuclei within the area was counted, and the total area was divided by the number of nuclei to give the average apical area per cell. To image in the XZ plane, Z-stacks were collected at 0.25 μm steps with a Leica TCS SP2 AOBS Laser scanning spectral confocal microscope, projected and examined in section view.

Wound migration studies

Monolayer cell wounding assays were performed on 4-well Permanox plastic chamberslides (Nunc, Roskilde) as described (Roux et al., 2005) with the following modifications. Monolayers were rinsed before and after wounding. After removal of media, a P1000 pipette tip with suction was used to make wounds and take away detached cells in completely confluent monolayers. Wounds were imaged with a Nikon TS100 inverted microscope equipped with a Nikon DS camera immediately after initial wounding and 6 and 20 h later. To ensure that identical areas were imaged at the selected time points, multiple positioning marks were made on the culture plates. To determine migration areas, edges of the wounds were carefully traced with the polygon tool of ImageJ software. Areas at the two time points were then used to compute the percentage of wound closure during the test period.

Rac activity assay

Rac activity in MDCK cells was measured using the G-LISA absorbance based Rac1 activation assay kit (Cytoskeleton Inc.). MDCK cells were lysed in buffer provided by the manufacturer and clarified lysates were incubated in Rac-GTP-binding protein-coated wells. Following washes to remove non-specific binding, bound Rac1-GTP was detected using anti-Rac1 primary and HRP-linked secondary antibodies. The read-out was obtained at wavelength 490 nm.

Statistical analyses

For all experiments, means ± S.D. were calculated and statistical significance determined by performing unpaired two-tailed *t* tests using GraphPad Prism software, or online calculators for S.D., *t* test and *P* value.

RESULTS

PMP22 is palmitoylated at C85

To investigate whether PMP22 is palmitoylated, we used CSS-Palm 2.0 software, which predicts the likelihood of palmitoylation within an input amino acid sequence (Ren et al., 2008). Analysing the PMP22 sequence, C85 received a favourable palmitoylation score. To test whether PMP22 is palmitoylated at this site, we mutated C85S, a conservative change expected to preserve protein structure, and stably expressed normal mouse WT or C85S-PMP22 in MDCK type II cells. An HA epitope tag in the second extracellular loop of PMP22 was added for detection, as a tag in this position neither affects the processing nor the trafficking of the protein (Tobler et al., 1999). To detect palmitoylated proteins in our cell lines, we employed a non-radioactive method in which cells are metabolically labelled with the palmitic acid analogue 17-ODYA (Charron et al., 2009; Martin and Cravatt, 2009). ODYA is identical with palmitate except it contains a single-terminal alkyne group which can be reacted with a biotin-azide reporter via the Cu(I)-catalysed azide-alkyne [3+2] cycloaddition (i.e., click chemistry) (Martin and Cravatt, 2009). Proteins biotinylated via incorporated 17-ODYA can then be rapidly detected on Western blots with streptavidin-HRP (Figures 1B–1E). As a positive control for palmitoylation, we used Palm-YFP, which is identified with anti-GFP antibodies (Zacharias et al., 2002). Palm-YFP-expressing MDCK cells were metabolically labelled with 17-ODYA or its solvent DMSO (control) and Palm-YFP was immunoprecipitated from cell lysates, followed by click-labelling and immunoblotting (Figure 1B). The immunoprecipitated Palm-YFP displays both YFP and biotin-labelling in 17-ODYA but not in DMSO-treated cells (Figure 1B, top). To demonstrate that the 17-ODYA is linked via a labile thiolester bond, click-labelled Palm-YFP immunoprecipitates were treated with Tris (T) as a control, or with HN (Charron et al., 2009; Martin and Cravatt, 2009). HN hydrolyses thiolester bonds and leads to the disappearance of the Palm-YFP label, as compared with

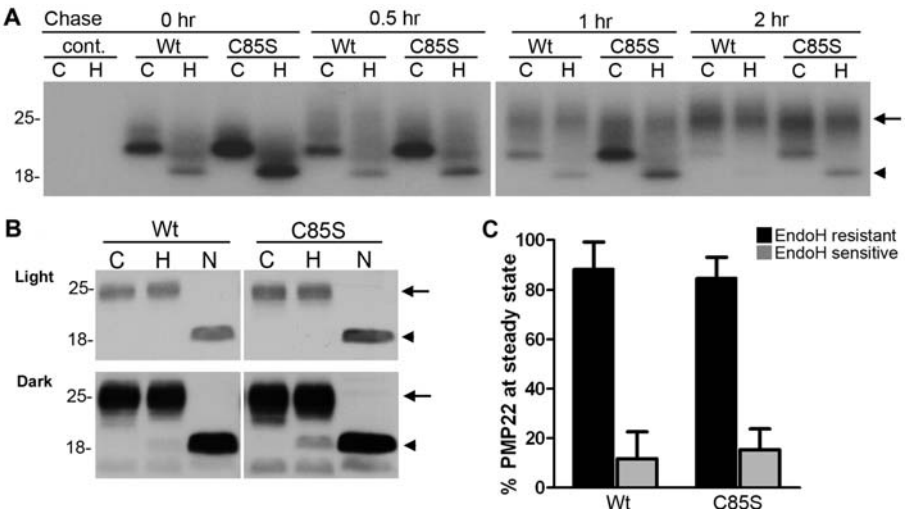

Figure 2 **Palmitoylation of PMP22 is not required for the maturation of the protein**
Parental control (cont.), WT- or C85S-PMP22 expressing MDCK cells were labelled with ^{35}S-methionine and cysteine for 30 min and then chased with unlabelled media for the indicated times (**A**). RIPA buffer-soluble extracts were immunoprecipitated with HA matrix, divided in half and incubated with (H) or without (**C**) Endo H. Endo H resistant PMP22 is marked with an arrow, while the Endo H-sensitive PMP22 is marked with an arrowhead. To assess the glycosylation of PMP22 at steady-state, total cell lysates (10 μg/reaction) were incubated without enzyme (C), or with Endo H (H) or PNGase F (N) and blotted with an anti-HA antibody (**B**). Light exposure (top panel) of the film shows mature Endo H-resistant PMP22 migrating at around 25 kDa (H, arrows), while the deglycosylated polypeptide resolves approximately 18 kDa (N, arrowheads). A dark exposure of the same blot (lower panel) detects Endo H-sensitive PMP22. Molecular mass, in kDa. Semi-quantitative analyses of five independent experiments reveal that over 80% of WT and C85S-PMP22 similarly achieve Endo H-resistance at steady-state (**C**).

Tris (Figure 1B bottom). This result signifies that the 17-ODYA label is S-bonded.

Control and WT- or C85S-PMP22 expressing MDCK cells were similarly labelled with 17-ODYA or its solvent DMSO and lysed in RIPA buffer for immunoprecipitation with anti-HA antibodies. RIPA buffer soluble (Figure 1C) and insoluble (Figure 1D) fractions were processed separately. Although both WT and C85S expressing cells immunoprecipitated PMP22, only WT-PMP22 showed HN-sensitive 17-ODYA labelling (Figures 1C and 1D). Furthermore, the majority of both WT- and C85S-PMP22 is detected within the RIPA buffer insoluble fraction, with approximately 90% of the palmitoylated PMP22 partitioning in this pool (Figure 1D). Compared with WT-PMP22 expressing cells, lysates from the C85S cultures contain a pronounced fast migrating fraction in the detergent-soluble pool (Figures 1C, arrowhead and 1D), likely indicating altered processing of the palmitoylation-deficient PMP22.

We also determined whether PMP22 acquires palmitoylation in Schwann cells which are the most robust site of PMP22 expression (Pareek et al., 1997). Primary cultures of rat Schwann cells transfected with the WT- or the C85S-PMP22 construct expressed the recombinant HA-tagged protein (Figure 1E). Consistent with the MDCK cells, only WT-PMP22 is 17-ODYA-labelled, as detected with biotin-HRP. The observed broad migration pattern of the recombinant protein seen in these experiments is consistent with the gel mobility of PMP22 from sciatic nerves, and is likely due to heterogeneity in the carbohydrate modification of the protein (Pareek et al., 1997). The mild reducing conditions required to protect the S-linked 17-ODYA label may have also contributed to PMP22 migrating as a smear (Figures 1C–1E). Together these results show that PMP22 acquires palmitoylation at C85 in both epithelial and glial cells, and mutating this cysteine to serine abolishes the palmitoylation of the protein.

Palmitoylation is not essential for the maturation of PMP22

As palmitoylation is known to affect the trafficking of membrane proteins through the secretory pathway (Franch-Marro et al., 2008), we compared the processing of WT and C85S-PMP22 by pulse-chase analyses using the MDCK culture model (Figure 2A). Our previous studies show that the majority of newly synthesized PMP22 is targeted for proteasomal degradation and only approximately 20% of the protein acquires complex carbohydrate modification which can be detected by resistance to Endo H (Pareek et al., 1997; Rangaraju et al., 2010). Indeed, at the 2 h chase time point, nearly all of the newly synthesized WT-PMP22 is Endo H resistant (~98%) (Figure 2A, arrow). In comparison, the C85S-PMP22 still contains a visible Endo H sensitive fraction (Figure 2A, arrowhead), which comprises approximately 15% of the total protein at 2 h. Therefore abolishing the palmitoylation of PMP22 slows the maturation of newly synthesized protein; however, it does not block its processing through the secretory pathway.

To corroborate the results of the pulse-chase experiments, we compared the glycosylation state of WT- and C85S-PMP22

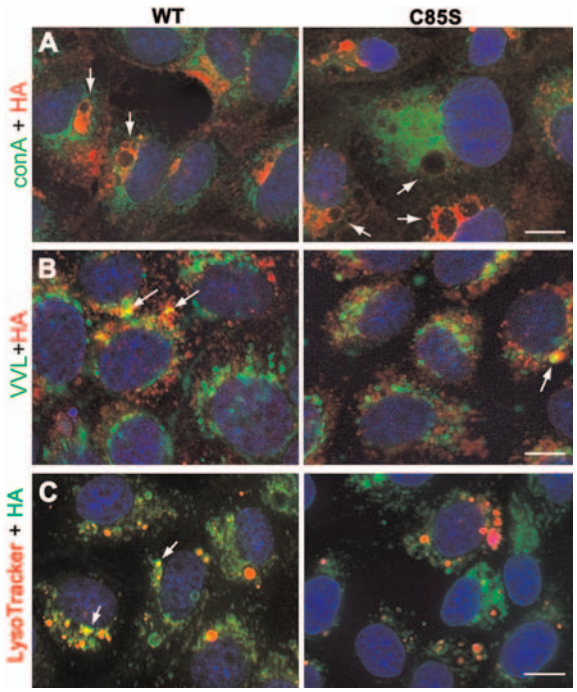

Figure 3 Palmitoylation-deficient PMP22 traffics through the secretory pathway, similar to WT

MDCK cells expressing WT- or C85S-PMP22 were fixed and immunolabelled with anti-HA antibodies and organelle markers after detergent permeabilization (**A–C**). In single plane confocal images, intracellular WT- and C85S-PMP22 (red) are often detected around vacuolar structures (arrows) that do not co-label with the ER marker ConA (green) (**A**). Intracellular WT- and C85S-PMP22 are seen in VVL (green) labelled Golgi compartments resulting in a few yellow spots (arrows) (**B**). LysoTracker (red) loaded cultures were stained with anti-HA and show that neither WT- nor C85S-PMP22 (green) overly co-localize with lysosomes (**C**). Vesicles with strong PMP22-like and LysoTracker co-labelling are marked with arrows. Nuclei are stained with Hoechst dye (blue) (**A–C**). Scale bar, 10 μm.

at steady-state (Figure 2B). Total protein lysates of WT or C85S-PMP22 expressing MDCK cells were treated with Endo H or PNGase F, which removes all N-linked carbohydrates from PMP22 (Pareek et al., 1997). As shown on the anti-HA Western blots, the majority of both WT- and C85S-PMP22 is resistant to Endo H digestion, and shifts to approximately 18 kDa migration position upon PNGase F treatment (Figure 2B, arrowhead). A dark exposure of the same blot reveals the Endo H sensitive fraction in the samples, with a more prominent band in the C85S-PMP22, as compared with WT (Figure 2B, arrowhead). Nonetheless, semi-quantitative analyses of five independent experiments did not detect a statistically significant difference between the cell lines and indicate that over 80% of WT and C85S-PMP22 similarly acquire Endo H resistance at steady-state (Figure 2B and 2C).

We also examined the trafficking of WT and C85S-PMP22 through the secretory pathway using organelle markers and confocal microscopy (Figure 3). As suggested by the biochemical studies (Figure 2), neither WT- nor C85S-PMP22 is retained in the ER (endoplasmic reticulum), which we identified with the lectin, Con A (Figure 3A, green). On single plane confocal images, large intracellular PMP22-positive vacuoles (detected by HA-reactivity) are prominent in both WT- and C85S-PMP22 expressing cells (Figure 3A arrows). Cells were also co-stained for PMP22 and VVL, a Golgi marker (Figure 3B, green). In agreement with the processing of PMP22 through the Golgi compartment and the resistance of the protein to Endo H at steady-state (Pareek et al., 1997) (Figure 2), some anti-HA positive structures in both WT and C85S-PMP22 co-localize with VVL (Figure 3B, arrows). Additionally, the cultures were reacted with anti-HA antibody after loading with Lysotracker Red, a dye that is taken up by acidic compartments such as lysosomes in living cells. Neither WT nor C85S-PMP22 accumulates in Lysotracker-positive vesicles, unless the expression of the recombinant protein is very high (Figure 3C, arrows). Together these results indicate that deletion of the C85 palmitoylation site in PMP22 does not significantly impact the intracellular processing of the protein, as compared with WT.

WT and C85S are targeted to the plasma membrane and influence the distribution of apical membrane proteins

MDCK cells form polarized monolayers where the targeting of proteins to the basolateral and apical membranes can be examined (Kroepfl and Gardinier, 2001). Our previous studies in these cells showed the localization of endogenous PMP22 at intercellular junctions and alteration in monolayer permeability upon overexpression of human WT-PMP22 (Notterpek, 2001; Roux et al., 2005). To investigate the effect of palmitoylation on the targeting of PMP22 to the plasma membrane, we immunostained WT and C85S-PMP22 MDCK cultures without permeabilization (Vega-Salas et al., 1987; Charron et al., 2009) (Figures 4A and 4B). Cell surface PMP22 is accessible using antibodies to the HA epitope tag which is located in the second extracellular loop of the protein (Tobler et al., 1999). In WT-PMP22 expressing cultures, the HA-like staining appears speckled with a ring-like pattern in many of the cells (Figure 4A left panel, arrows). As a control of specificity for the immunostaining, cells that stably express the empty vector (V) yielded low reactivity after incubation with the HA antibody (Figure 4A′). In C85S-PMP22 expressing cells, the HA-like immunoreactivity is rather uniform with some focal concentrations (Figure 4A, C85S, arrowheads) and only occasional ring-like pattern (arrow). To confirm the localization of PMP22 to the apical membrane, non-permeabilized cells were first reacted with the anti-HA antibody and subsequently treated with detergent and incubated with an antibody to the apical marker GP135/podocalyxin (Ojakian and Schwimmer, 1994) (Figure 4B). Using this approach, we detected a notable co-localization of WT and C85S-PMP22 with GP135 (Figure 4B). In addition, when imaged under identical conditions, we observed intensified GP135-like immunoreactivity in both WT- and C85S-PMP22 cultures as compared with vector control (Figure 4C). In comparison, the expression and the distri-

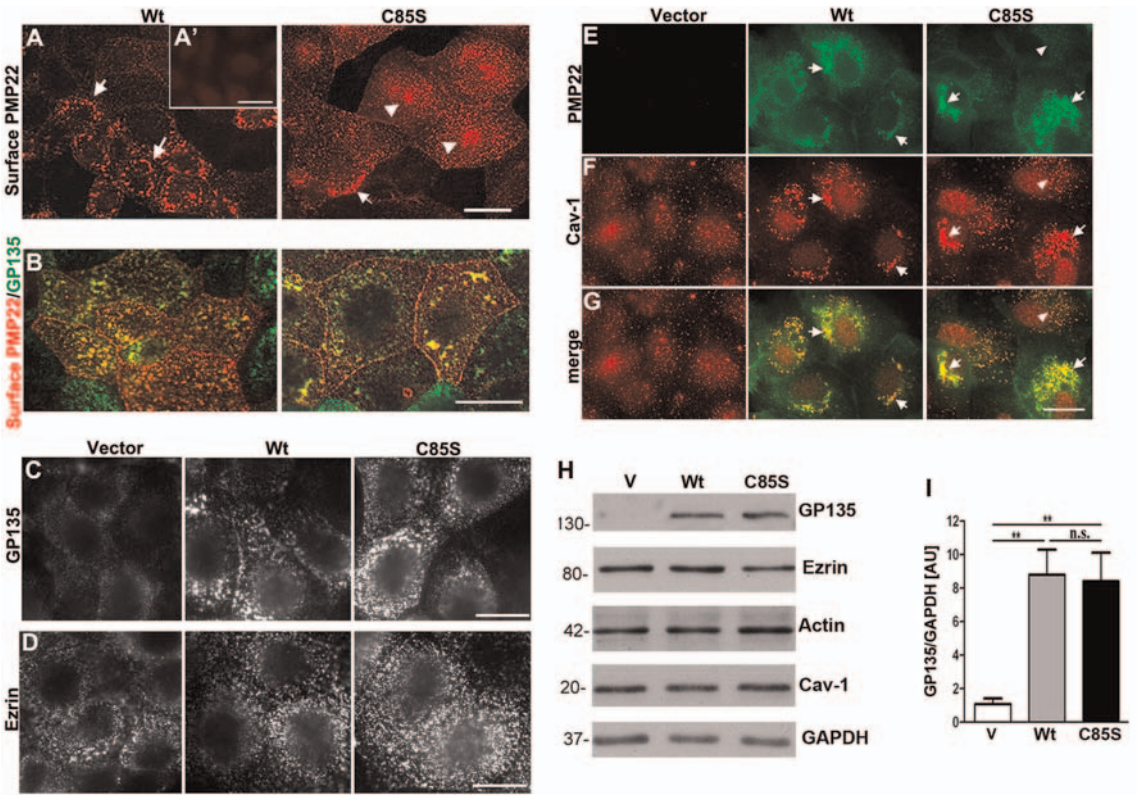

Figure 4 **Palmitoylation of PMP22 influences the cell surface distribution of the protein, and overexpression of WT- or C85S-PMP22 impact the levels of GP135 and the localization of caveolin**

Non-permeabilized MDCK cultures were immunolabelled with anti-HA antibodies to detect PMP22 on the cell surface (**A**, **B**). WT-PMP22 is detected in clustered puncta which are often arranged in ring-like patterns (arrows). In C85S cells, PMP22-like distribution is more diffuse, with some clustering (arrowheads). Anti-HA-like immunoreactivity is absent in vector only MDCK cells (**A′**, inset). Endogenous apical proteins GP135 (**B**, **C**) and ezrin (**D**) have similar distribution patterns between WT- and C85S-PMP22 cells, and show partial co-localization with PMP22 (**B**). When imaged for the same exposure times, PMP22 overexpressing cells show elevated levels of GP135-like staining (**C**), while ezrin appears unaffected (**D**). In permeabilized cells, intracellular PMP22 (green) is extensively co-localized with caveolin-1 (red) positive vesicles, which appear larger and more clustered when PMP22 is overexpressed (arrows in **E**–**G**), as compared with non-expressing cells (arrowhead in **E** and vector panels). Scale bar, 10 μm (**A**–**G**). Biochemical analyses of apical proteins demonstrate a pronounced elevation of GP135 in WT and C85S-PMP22 cells relative to vector controls, whereas the levels of ezrin, actin and caveolin-1 are not affected (**H**). GAPDH is shown as a loading control. Semi-quantitative analyses of four independent experiments reveal a nearly 7-fold increase in GP135 in both WT and C85S-PMP22 cells, as compared with vector (V) control (**I**). Unpaired Student's *t* test; $^{**}P<0.01$; n.s.=non-significant.

bution of another apical membrane protein ezrin, which links actin filaments to the plasma membrane (Louvet-Vallee, 2000) did not appear to be affected by the overexpression of PMP22 (Figure 4D). Ezrin-like staining appears in fine speckles similarly in WT- and C85-PMP22 cultures (Figure 4D).

To determine whether the palmitoylation of PMP22 affects the distribution of the protein with respect to lipid-rich microdomains (Erne et al., 2002) we co-immunostained cells with anti-HA and anti-caveolin 1 antibodies (Figures 4E–4G). In permeabilized cells, WT- and C85-PMP22 are extensively co-localized with caveolin-1 yielding yellow colour on merged images (Figure 4G). Furthermore, we noticed a redistribution of caveolin-1 between vector control and PMP22 expressing cells. Whereas caveolin-1 is distributed throughout the cells in non-transduced and vector control cultures (Figures 4E–4G, arrowheads), the overexpression of PMP22 leads to clustering of caveolin-reactive microdomains (Figures 4E–4G, arrows).

To corroborate the findings from the immunolocalization studies, next we assessed the expression of the studied apical proteins in lysates of vector control, WT- and C85-PMP22 cultures (Figure 4H). In agreement with the immunolabelling studies (Figure 4C), Western blot analyses show the up-regulation of GP135 in WT- and C85S-PMP22 cells as compared with vector control (Figure 4H). In contrast, we did not detect notable changes in the levels of ezrin, actin or caveolin in response to PMP22 overexpression. Semi-quantitative analyses of six independent experiments demonstrate a nearly 7-fold increase in GP135 levels in WT- and C85-PMP22 cultures as compared with vector controls (Figure 4I). These results indicate that although palmitoylation is not required for apical targeting of PMP22, the distribution and levels of certain apical proteins are impacted by the overexpression of PMP22, with discernible differences between WT and C85S.

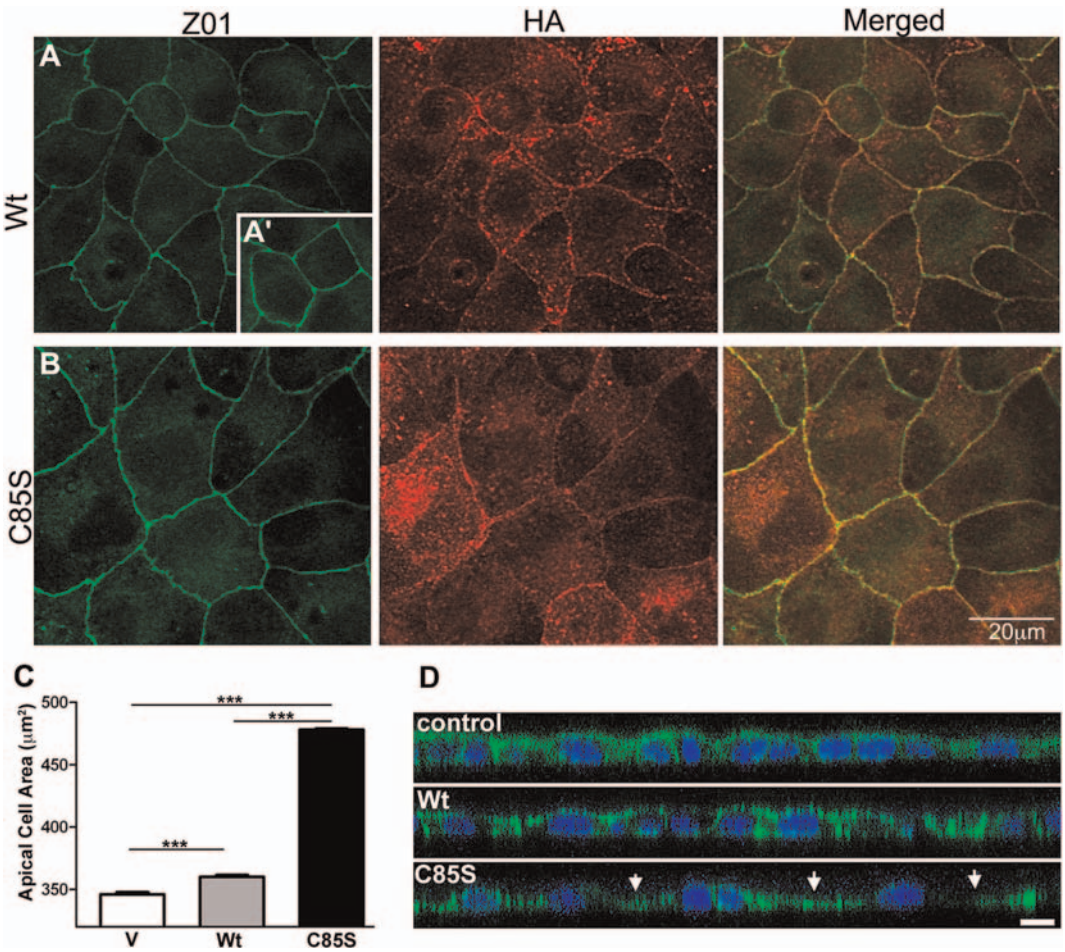

Figure 5 **Palmitoylation-deficient PMP22 is detected at intercellular junctions and is associated with an increase in apical cell area**
Permeabilized MDCK cultures were double immunolabelled with anti-HA (PMP22, red) and ZO1 (green) antibodies and imaged by confocal microscopy (**A**, **B**). ZO1 delineates the intercellular junctions and reveals expanded cell boundaries in C85S-PMP22, as compared with WT. Both WT- and C85S-PMP22 partially co-localize with ZO1 (**A**, **B**; merged). Inset in (**A**) shows ZO1-like staining in vector control cells. Quantification of apical areas measured from ZO1 immunostaining demonstrates apical area expansion in WT (n=430) and C85S-PMP22 expressing (n=407) cells, as compared with vector (V) (n=432) control (**C**). Unpaired Student's t test ***$P<0.001$. Confocal X–Z-plane images of control, WT- and C85S-PMP22 expressing MDCK cultures after staining with actin-phalloidin (green) (**D**). Nuclei are labelled with Hoechst dye. C85S monolayers are irregular with cells spaced far apart and thinned between nuclei (arrows). Scale bar, 10 μm.

Palmitoylation of PMP22 impacts epithelial cell morphology and migration

In MDCK epithelia, PMP22 is a constituent of tight junctions and overexpression of the human WT protein leads to expansion of the apical cell surface and flattened morphology (Notterpek, 2001; Roux et al., 2005). To examine if palmitoylation impacts the junctional targeting of PMP22 or its influence on cell shape, WT and C85S cells were co-stained for PMP22 and zonula occludins (ZO-1), a recognized junctional protein (Figure 5). As displayed on the single plane confocal images, both WT- and C85S-PMP22 are co-localized with ZO-1 at intercellular junctions (Figures 5A and 5B) indicating that the palmitoylation state of PMP22 is not crucial for targeting the protein to these sites. In agreement with our previous experiments with the human WT-PMP22 (Roux et al., 2005), overexpression of the mouse PMP22 is associated with an increase in the apical cell surface as compared with vector controls (Figures 5A, 5A′ and 5C). Notably, the apparent apical cell area is further increased in C85S-PMP22 cells in comparison with WT (Figures 5A and 5B). To quantify this effect, confluent MDCK monolayers were immunostained with anti-ZO1 antibody and the apical areas were assessed. Measurements in over 400 cells per condition revealed a nearly 30% increase in apical area upon overexpression of C85S-PMP22, as compared with vector control (Figure 5C). The expanded apical area of C85S cells could be due to a flattened morphology, as seen before in human WT-PMP22 cultures (Roux et al., 2005), or a gross increase in overall cell dimensions. To evaluate cell height, confluent monolayers stained for filamentous actin were imaged in the XZ plane

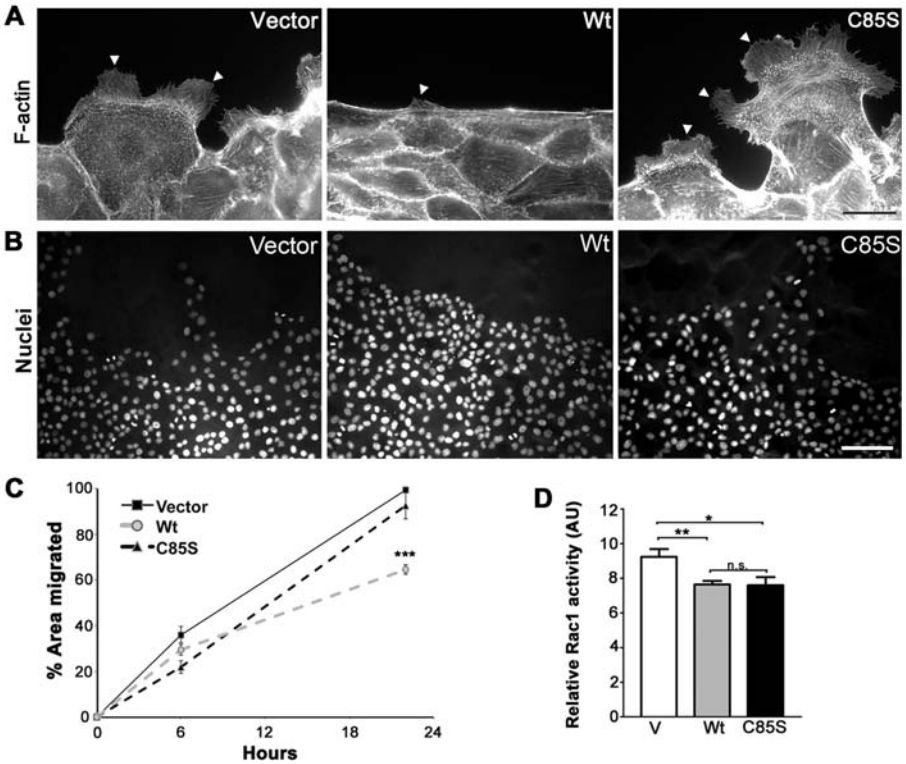

Figure 6 **Palmitoylation of PMP22 slows cell migration during wound closure**
Protrusive activity and distribution of actin were examined along the wound edge 24 h postwounding (**A**). Cultures stained with phalloidin to detect F-actin reveal lamellipodial extensions of the plasma membrane (arrowheads). Scale bar, 20 μm. Images of nuclei at and near the wound edges reveal that WT cells remain compact and resist spreading into the wounded area (**B**). Nuclei are labelled with Hoechst dye. Scale bar, 85 μm. The extent of migration of vector, WT- and C85S-PMP22 overexpressing cells were analysed after 6 and 20 h of the initial wounding (**C**). Quantification of percentage area migrated for each cell line from at least three independent experiments indicates that palmitoylation of PMP22 is associated with increased resistance to migration. Unpaired Student's *t* test ***$P<0.001$; n.s.= non-significant. Rac1 activity for each cell line was measured using a colorimetric assay and values from four independent experiments were plotted, with respect to the positive control (**D**). Unpaired Student's *t* test *$P<0.05$; **$P<0.005$; n.s.= non-significant. V, vector control; AU, arbitrary units.

(Figure 5D). Control and WT-PMP22 expressing monolayers display relatively even heights while the C85S monolayer shows thinning, and a rolling hill-like morphology, with peaks over the nuclei and valleys in between (Figure 5D, arrows). Thus, the increased apical area of C85S cells is associated with morphological changes in spreading and flattening.

Another important aspect of epithelial biology modulated by PMP22 is cell migration, which can be assessed by the capacity of monolayers to heal after wounding (Roux et al., 2005). Epithelial cells form an actin belt along the wound edge and leader cells extend lamellipodia and actively draw the monolayer forward to close the wound (Fenteany et al., 2000; Du et al., 2010). Concurrently, cells at the wound edge, and several layers deep, flatten and spread out as lamellipodial crawling proceeds. In such a wound-migration assay, human WT-PMP22 expressing MDCK cells closed wounds approximately 60% slower than controls and displayed reduced lamellipodial protrusions (Roux et al., 2005). Using the same cell migration assay, we find that when the cultures were stained with the F-actin marker, phalloidin, WT-PMP22 expressing cells display a nearly uninterrupted actin purse-string along the wound edge and only few lamellipodial protrusions (Figure 6A, arrowhead). In contrast, C85S and control cultures contain leader cells with lamellipodial protrusions, as they migrate to close the wound (Figure 6A, arrowheads). In agreement, when nuclei in wounded monolayers are visualized, WT cultures appear compact at the wound edge, while C85S cells spread out as effectively as vector controls (Figure 6B). To quantify these observed differences, we analysed MDCK cell migration 6 and 20 h after wounding (Figure 6C). Consistent with the morphological observations, mouse WT-PMP22 expressing cultures are slow to migrate as compared with vector control. In contrast, C85S-PMP22 cultures close wounds quite efficiently, showing no slowing relative to vector control (Figure 6C). Rho-like GTPases which include Rac1 have been identified as key regulators of epithelial architecture and cell migration (Sander and Collard, 1999). As both lamellipodial formation and cell migration are substantially decreased in wounded WT monolayers (Figures 6A–6C), we hypothesized that Rac1 activity may be inhibited either directly or indirectly by overexpressed WT-PMP22. To test this, we

measured Rac1 activity in vector control, WT-PMP22 and C85S-PMP22 expressing cultures using a commercial assay kit. Indeed, Rac 1 activity is reduced by approximately 18% when PMP22 is overexpressed, and this result is consistent among multiple independent experiments with WT and C85S cultures (Figure 6D). However, since lamellipodia morphology and migratory behaviour are normal when C85S-PMP22 is overexpressed, downstream effectors of Rac1 activity may be differentially affected by the palmitoylation of PMP22. Together these results suggest that the palmitoylation state of PMP22 is a critical determinant in modulating the interactions of the protein with molecules influencing epithelial cell migration.

DISCUSSION

In this study, we show that mouse PMP22 is palmitoylated at C85 and mutating C85S abolishes PMP22 palmitoylation. We further demonstrate that the palmitoylation state of PMP22 impacts the trafficking and function of the protein in MDCK cells. While at steady-state both WT and C85S-PMP22 acquire >80% resistance to Endo H digestion, by pulse-chase analyses we detect slower maturation of the mutant protein as compared with WT. We find that in polarized epithelia WT- and C85S-PMP22 sort differently at the apical plasma membrane and partially co-localize with GP135 and caveolin. The overexpression of WT- or C85S-PMP22 similarly increases the levels of GP135 and alters the localization of caveolin. Additionally, WT and C85S cultures display morphological differences at confluence with C85S cells appearing apically expanded and flattened. In a wound-migration assay, WT cells resist changing morphology or migrating, while C85S cells perform similarly to vector controls. Overall, these data indicate that while palmitoylation of PMP22 is not essential for targeting the protein to the plasma membrane, it favours the maintenance of a compact, stable monolayer.

Post-translational modification is critical for the functioning of membrane proteins, yet for PMP22 this aspect has not been investigated in detail. Previously, we found that glycosylation at asparagine 41 was not essential for trafficking PMP22 to the plasma membrane; however, it had an influence on PMP22 oligomer stability (Ryan et al., 2000). Palmitoylation has recently emerged as a reversible post-translational modification that can influence the trafficking of proteins between membrane compartments (Linder and Deschenes, 2007). In polarized cells, such as neurons and myelinated glia, the correct and dynamic trafficking of proteins to specific membrane domains is critical for basic function (Fukata and Fukata, 2010). While a large number of palmitoylated neuronal proteins have recently been identified, with regard to glial biology this modification has been less studied. As lipid modifications, such as palmitoylation, increase the hydrophobicity of proteins, it is highly likely that palmitoylated proteins are abundant in myelinated glial cells. Indeed, myelin protein zero (P0), which constitutes approximately 50% of the total protein in peripheral nerve myelin was shown to be palmitoylated at cysteine 153 (Bizzozero et al., 1994; Melendez and Bizzozero, 1996). More recently, it was reported that palmitoylation of P0 peptides increases the immunogenicity of the protein, suggesting a role in immune-mediated disorders of the peripheral nervous system (Beaino and Trifilieff, 2010). While we have not investigated how palmitoylation influences the functioning of PMP22 in peripheral nerves, there are two human neuropathy-associated mutations (L80P, L82P) (Tyson et al., 1997) that dramatically decrease the palmitoylation score for C85 from high (likely) to low (unlikely). This data raises the possibility that these mutations impact nerve health via a negative effect on PMP22 palmitoylation.

Besides being a hydrophobic tetraspan membrane protein, and the conservation of C85 across species (Figure 1), PMP22 has other properties that suggest a critical role for palmitoylation in regulating the activity of this disease-linked molecule. As mentioned above, PMP22 forms homodimers and larger oligomers (Tobler et al., 2002), which could be regulated by palmitoylation (Kovalenko et al., 2004). Furthermore, PMP22 is an aggregation-prone proteasome substrate that accumulates in cytosolic aggregates when the proteasome is inhibited or the protein is overproduced (Fortun et al., 2006; Tobler et al., 1999). While the specific site(s) of ubiquitination have not been identified, accumulation of poly-ubiquitinated PMP22 is detected in cells after proteasome inhibition (Fortun et al., 2005). As palmitoylation has been shown to prevent the ubiquitylation of proteins (Linder and Deschenes, 2007) it is possible that the subcellular fate of PMP22, at least in part, is regulated by dynamic interactions between these two pathways. Interestingly, our pulse-chase studies did not detect increased degradation of the palmitoylation-deficient PMP22, but rather showed an extended half-life of the Endo H-sensitive C85S protein, as compared with WT (Figure 2). This finding indicates slowed trafficking and/or recycling of C85S-PMP22 between the early-Golgi and ER compartments, which are check points for PMP22 protein quality control (Pareek et al., 1997; Sanders et al., 2001).

The interpretation of the results presented in this article is limited by the fact that we used the MDCK cell model, rather than primary Schwann cells. The rationale for taking this approach stems from previous reports that have proposed an analogy between the apical and basolateral domains of epithelial cells and compact and non-compact myelin, respectively (Kroepfl and Gardinier, 2001). For instance, PLP (proteolipid protein), a component of compact myelin in oligodendrocytes, is targeted apically in MDCK cells (Kroepfl and Gardinier, 2001). Furthermore, molecular control of polarization in peripheral nerve myelin has been shown to be similar to that in epithelial cells (Ozcelik et al., 2010). In addition, while overexpression of PMP22 can induce cell death and membrane blebbing in Schwann cells (Fabbretti et al., 1995), in MDCK cells we found a remarkably efficient maturation of the exogenous mouse protein (Figures 2 and

3). Using this model allowed us to detect PMP22 on the apical membrane in non-permeabilized MDCK cells, which is also the site for proteolipid protein targeting (Kroepfl and Gardinier, 2001). Since both PMP22 and PLP are tetraspan protein components of compact myelin (Bronstein, 2000), this finding further validates the use of polarized epithelia for studies of myelin protein trafficking.

A somewhat surprising finding in our studies concerns the efficient trafficking of palmitoylation-deficient PMP22 to the plasma membrane (Figures 3–5). This is in contrast with findings in cultured oligodendrocytes, where palmitoylation regulates the sorting of proteins to specific membrane domains (Schneider, 2005). In co-cultures of neurons and oligodendrocytes, palmitoylated proteins were translocated into myelin-like membranes while a palmitoylation-deficient PLP mutant did not target efficiently to these sites. Similarly, another tetraspan protein claudin-14, was less efficiently localized to specific membrane domains when palmitoylation was abolished by site-directed mutagenesis (Van Itallie, 2005). In our approach, instead of using a chemical method to block palmitoylation in general, we used site-directed mutagenesis to selectively prevent the palmitoylation of PMP22. While we did not detect pronounced differences in the localization of WT- or C85S-PMP22 in the major organelles, the distribution of the exogenous proteins on the apical plasma membrane is distinct. As palmitoylated proteins tend to associate with each other and are found in lipid rafts (Zacharias et al., 2002), it is likely that this lipid modification influences the interaction of PMP22 within the plasma membrane either by association with rafts, or with other hydrophobic or palmitoylated proteins. Differences in the distribution of WT- and C85S-PMP22 at the plasma membrane could also influence functionality and downstream signalling. Up-regulation of GP135 but not ezrin (Figure 4) suggests that PMP22 is involved in regulating GP135 expression in MDCK cells. GP135 establishes a preapical domain in single MDCK cells, and its down-regulation causes defects in polarization (Meder, 2005). As our evidence indicates that PMP22 is upstream of GP135, it may also be a regulator of these processes. In addition, GP135 is the canine orthologue of human podocalyxin, involved in formation of podocytes in the kidney, and a malignancy marker in a variety of cancers (Hsu et al., 2010). PMP22 has also been implicated in cancer, raising the possibility that PMP22 could influence GP135/podocalyxin expression in some types of tumours.

How might the palmitoylation state of PMP22 alter the morphology and migrational status of cells from a mechanistic perspective? Concerning cell morphology, WT cells in confluent monolayers are compact whereas C85S cells are spread out and resist adopting a compact morphology (Figures 4–6). These results suggest that palmitoylated PMP22 is involved in the efficient transition from a polygonal, flat morphology to a compact, columnar shape at confluence. Furthermore, the wound-healing assay shows that C85S cells are quite able to spread out and migrate across the wounded area, while WT cells resist doing so (Figure 6). The inhibitory activity of WT-PMP22 on lamellipodial protrusion and cell migration, in part are likely driven by inhibition of Rac1 at the plasma membrane, yet both WT- and C85S-PMP22 similarly inhibit Rac1 activity, and increase the expression of GP135 (podocalyxin) an indirect Rac1 regulatory protein (Schmieder, 2004; Hsu et al., 2010). This finding suggests that the palmitoylation state of PMP22 impacts the interaction(s) of the protein with other signalling pathways that influence the migratory behaviour of epithelia. Besides affecting Rac1 activity, another plausible way WT-PMP22 might affect these processes is through interaction with occludin, a tetraspan tight junction protein recently shown to regulate epithelial migration (Du et al., 2010). Occludin knockdown decreased formation of lamellipodia at the wound edge in MDCK cultures and increased the actin belt. Endogenous canine PMP22 is co-expressed with occludin at apical intercellular junctions in MDCK cells (Notterpek, 2001), which raises the possibility that palmitoylated PMP22 may affect occludin at the junctions and interfere with its activity.

In summary, based on these findings it will be important to investigate whether palmitoylation affects the trafficking, targeting, or function of PMP22 within Schwann cells and myelin. Particularly, in light of known disease-causing PMP22 mutations near the palmitoylation site (Tyson et al., 1997) advancing the understanding of PMP22 lipid modifications will likely provide insights into conditions that centre on PMP22 dysfunction.

ACKNOWLEDGEMENTS

We are grateful to members of the Notterpek laboratory for insightful discussions, Doug Smith for help with the confocal microscopy and Kelli Fraga for assistance with generating the C85S mutation.

FUNDING

These studies were supported, in part, by the US National Institutes of Health [grant number NS041012] and the McKnight Brain Institute of the University of Florida.

REFERENCES

Adlkofer K, Martini R, Aguzzi A, Zielasek J, Toyka KV, Suter U (1995) Hypermyelination and demyelinating peripheral neuropathy in PMP22-deficient mice. Nat Genet 11:274–280.

Amici SA, Dunn WA, Notterpek L (2007) Developmental abnormalities in the nerves of peripheral myelin protein 22-deficient mice. J Neuroscie Res 85:238–249.

Aston C, Jiang L, Sokolov BP (2004) Transcriptional profiling reveals evidence for signaling and oligodendroglial abnormalities in the temporal cortex from patients with major depressive disorder. Mol Psychiatry 10:309–322.

Beaino W,Trifilieff E (2010) Thiopalmitoylated peptides from the peripheral nervous system myelin p0 protein: synthesis, characterization, and neuritogenic properties. Bioconjug Chem 21:1439–447.

Bizzozero OA, Fridal K, Pastuszyn A (1994) Identification of the palmitoylation site in rat myelin P0 glycoprotein. J Neurochem 62:1163–1171.

Brancolini C, Marzinotto S, Edomi P, Agostoni E, Fiorentini C, Muller HW, Schneider C (1999) Rho-dependent regulation of cell spreading by the tetraspan membrane protein Gas3/PMP22. Mol Biol Cell 10:2441–2459.
Bronstein JM (2000) Function of tetraspan proteins in the myelin sheath. Curr Opin Neurobiol 10:552–557.
Charron G, Zhang MM, Yount JS, Wilson J, Raghavan AS, Shamir E, Hang HC (2009) Robust fluorescent detection of protein fatty-acylation with chemical reporters. J Am Chem Soc 131:4967–4975.
Dracheva S, Davis KL, Chin B, Woo DA, Schmeidler J, Haroutunian V (2006) Myelin-associated mRNA and protein expression deficits in the anterior cingulate cortex and hippocampus in elderly schizophrenia patients. Neurobiol Dis 21:531–540.
Du D, Xu F, Yu L, Zhang C, Lu X, Yuan H, Huang Q, Zhang F, Bao H, Jia L (2010) The tight junction protein, occludin, regulates the directional migration of epithelial cells. Dev Cell 18:52–63.
Erne B, Sansano S, Frank M, Schaeren-Wiemers N (2002) Rafts in adult peripheral nerve myelin contain major structural myelin proteins and myelin and lymphocyte protein (MAL) and CD59 as specific markers. J Neurochem 82:550–562.
Fabbretti E, Edomi P, Brancolini C, Schneider C (1995) Apoptotic phenotype induced by overexpression of wild-type gas3/PMP22: its relation to the demyelinating peripheral neuropathy CMT1A. Genes Dev 9:1846–1856.
Fenteany G, Janmey PA, Stossel TP (2000) Signaling pathways and cell mechanics involved in wound closure by epithelial cell sheets. Curr Biol 10:831–838.
Fortun J, Go J, Li J, Amici S, Dunnjr W, Notterpek L (2006) Alterations in degradative pathways and protein aggregation in a neuropathy model based on PMP22 overexpression. Neurobiol Dis 22:153–164.
Fortun J, Li J, Go J, Fenstermaker A, Fletcher BS, Notterpek L (2005) Impaired proteasome activity and accumulation of ubiquitinated substrates in a hereditary neuropathy model. J Neurochem 92:1531–1541.
Franch-Marro X, Wendler F, Griffith J, Maurice MM, Vincent JP. (2008) *In vivo* role of lipid adducts on Wingless. J Cell Sci 121:1587–1592.
Fukata Y, Fukata M (2010) Protein palmitoylation in neuronal development and synaptic plasticity. Nat Rev Neurosci 11:161–175.
Greaves J, Chamberlain LH (2007) Palmitoylation-dependent protein sorting. J Cell Biol 176:249–254.
Hemler ME (2003) Tetraspanin proteins mediate cellular penetration, invasion, and fusion events and define a novel type of membrane microdomain. Annu Rev Cell Dev Biol 19:397–422.
Hobbs S, Jitrapakdee S, Wallace JC (1998) Development of a bicistronic vector driven by the human polypeptide chain elongation factor 1alpha promoter for creation of stable mammalian cell lines that express very high levels of recombinant proteins. Biochem Biophys Res Commun 252:368–372.
Houlden H, Reilly MM (2006) Molecular genetics of autosomal-dominant demyelinating Charcot-Marie-Tooth disease. Neuromol Med 8:43–62.
Hsu YH, Lin WL, Hou YT, Pu YS, Shun CT, Chen CL, Wu YY, Chen JY, Chen TH, Jou TS (2010) Podocalyxin EBP50 ezrin molecular complex enhances the metastatic potential of renal cell carcinoma through recruiting rac1 guanine nucleotide exchange factor ARHGEF7. Am J Pathol 176:3050–3061.
Huhne K, Park O, Liehr T, Rautenstrauss B (1999) Expression analysis of the PMP22 gene in glioma and osteogenic sarcoma cell lines. J Neurosci Res 58:624–631.
Johnson JS, Roux KJ, Fletcher BS, Fortun J, Notterpek L (2005) Molecular alterations resulting from frameshift mutations in peripheral myelin protein 22: implications for neuropathy severity. J Neurosci Res 82:743–752.
Kovalenko OV, Yang X, Kolesnikova TV, Hemler ME (2004) Evidence for specific tetraspanin homodimers: inhibition of palmitoylation makes cysteine residues available for cross-linking. Biochem J 377:407–417.
Kroepfl JF, Gardinier MV (2001) Mutually exclusive apicobasolateral sorting of two oligodendroglial membrane proteins, proteolipid protein and myelin/oligodendrocyte glycoprotein, in Madin–Darby canine kidney cells. J Neurosci Res 66:1140–1148.
Le-Niculescu H, Kurian SM, Yehyawi N, Dike C, Patel SD, Edenberg HJ, Tsuang MT, Salomon DR, Nurnberger JI, Niculescu AB (2008) Identifying blood biomarkers for mood disorders using convergent functional genomics. Mol Psychiatry 14:156–174.
Li J, Kleeff J, Exposito I, Kayed H, Felix K, Giese T, Buchler M.W., Friess H (2005) Expression analysis of PMP22/Gas3 in premalignant and malignant pancreatic lesions. J Histochem Cytochem 53:885–893.
Linder ME, Deschenes RJ (2007) Palmitoylation: policing protein stability and traffic. Nat Rev Mol Cell Biol 8:74–84.
Louvet-Vallee S (2000) ERM proteins: from cellular architecture to cell signaling. Biol Cell 92:305–316.
Martin BR, Cravatt BF (2009) Large-scale profiling of protein palmitoylation in mammalian cells. Nature Methods 6:135–138.
Meder D (2005) Gp135/podocalyxin and NHERF-2 participate in the formation of a preapical domain during polarization of MDCK cells. J Cell Biol 168:303–313.
Melendez RF, Bizzozero OA (1996) Palmitoylation of myelin P0 protein is independent of its synthesis and parallels that of phospholipids. Journal of the peripheral nervous system: JPNS 1:34–41.
Mimori K, Kataoka A, Yoshinaga K, Ohta M, Sagara Y, Yoshikawa Y, Ohno S, Barnard GF, Mori M (2005) Identification of molecular markers for metastasis-related genes in primary breast cancer cells. Clin Exp Metastasis 22:59–67.
Notterpek L (2001) Peripheral myelin protein 22 is a constituent of intercellular junctions in epithelia. Proc Natl Acad Sci USA 98:14404–14409.
Ojakian GK, Schwimmer R (1994) Regulation of epithelial cell surface polarity reversal by beta 1 integrins. J Cell Sci 107:561–76.
Ozcelik M, Cotter L, Jacob C, Pereira JA, Relvas JB, Suter U, Tricaud N (2010) Pals1 is a major regulator of the epithelial-like polarization and the extension of the myelin sheath in peripheral nerves. J Neurosci 30:4120–4131.
Pareek S, Notterpek L, Snipes GJ, Naef R, Sossin W, Laliberte J, Iacampo S, Suter U, Shooter EM, Murphy RA. (1997) Neurons promote the translocation of peripheral myelin protein 22 into myelin. J Neurosci 17:7754–7762.
Rangaraju S, Verrier JD, Madorsky I, Nicks J, Dunn WA Jr, Notterpek L (2010) Rapamycin activates autophagy and improves myelination in explant cultures from neuropathic mice. J Neurosci 30:11388–11397.
Ren J, Wen L, Gao X, Jin C, Xue Y, Yao X (2008) CSS-Palm 2.0: an updated software for palmitoylation sites prediction. Protein Eng Des Sel 21:639–644.
Roux KJ, Amici SA, Fletcher BS, Notterpek L. (2005) Modulation of epithelial morphology, monolayer permeability, and cell migration by growth arrest specific 3/peripheral myelin protein 22. Mol Biol Cell 16:1142–1151.
Roux KJ, Amici SA, Notterpek L (2004) The temporospatial expression of peripheral myelin protein 22 at the developing blood-nerve and blood-brain barriers. J Comp Neurol 474:578–588.
Ryan MC, Notterpek L, Tobler AR, Liu N, Shooter EM. (2000) Role of the peripheral myelin protein 22 N-linked glycan in oligomer stability. J Neurochem 75:1465–1474.
Sander EE, Collard JG (1999) Rho-like GTPases: their role in epithelial cell-cell adhesion and invasion. Eur J Cancer 35:1905–1911.
Sanders CR, Ismail-Beigi F, McEnery MW (2001) Mutations of peripheral myelin protein 22 result in defective trafficking through mechanisms which may be common to diseases involving tetraspan membrane proteins. Biochemistry 40:9453–9459.
Schmieder S (2004) Podocalyxin activates RhoA and induces actin reorganization through NHERF1 and ezrin in MDCK cells. J Am Soc Nephrol 15:2289–2298.
Schneider A (2005) Palmitoylation is a sorting determinant for transport to the myelin membrane. J Cell Sci 118:2415–2423.
Tobler AR, Liu N, Mueller L, Shooter EM (2002) Differential aggregation of the Trembler and Trembler J mutants of peripheral myelin protein 22. Proc Natl Acad Sci USA 99:483–488.
Tobler AR, Notterpek L, Naef R, Taylor V, Suter U, Shooter EM (1999) Transport of Trembler-J mutant peripheral myelin protein 22 is blocked in the intermediate compartment and affects the transport of the wild-type protein by direct interaction. J Neurosci 19:2027–2036.
Tyson J, Ellis D, Fairbrother U, King RH, Muntoni F, Jacobs J, Malcolm S, Harding AE, Thomas PK (1997) Hereditary demyelinating neuropathy of infancy. a genetically complex syndrome. Brain 120:47–63.
van Dartel M, Cornelissen PW, Redeker S, Tarkkanen M, Knuutila S, Hogendoorn PC, Westerveld A, Gomes I, Bras J, Hulsebos TJ (2002) Amplification of 17p11.2 approximately p12, including PMP22, TOP3A, and MAPK7, in high-grade osteosarcoma. Cancer Genet Cytogenet 139:91–96.
Van Itallie CM (2005) Palmitoylation of claudins is required for efficient tight-junction localization. J Cell Sci 118:1427–1436.
Vega-Salas DE, Salas PJ, Rodriguez-Boulan E (1987) Modulation of the expression of an apical plasma membrane protein of Madin–Darby canine kidney epithelial cells: cell–cell interactions control the appearance of a novel intracellular storage compartment. J Cell Biol 104:1249–1259.
Yang X (2004) Palmitoylation supports assembly and function of integrin–tetraspanin complexes. J Cell Biol 167:1231–1240.
Zacharias DA, Violin JD, Newton AC, Tsien RY (2002) Partitioning of lipid-modified monomeric GFPs into membrane microdomains of live cells. Science 296:913–916.

Zhou B, Liu L, Reddivari M, Zhang XA (2004) The palmitoylation of metastasis suppressor KAI1/CD82 is important for its motility- and invasiveness-inhibitory activity. Cancer Res 64:7455–7463.

Zoltewicz JS, Ashique AM, Choe Y, Lee G, Taylor S, Phamluong K, Solloway M, Peterson AS, Ruhrberg C (2009) Wnt signaling is regulated by endoplasmic reticulum retention. PLoS ONE. 4:e6191.

Received 26 June 2012/1 November 2012; accepted 5 November 2012

Published as Immediate Publication 5 November 2012, doi 10.1042/AN20120045